A Search for Light Dark Matter Interactions Enhanced by the Migdal effect or Bremsstrahlung in XENON1T

E. Aprile,[1] J. Aalbers,[2] F. Agostini,[3] M. Alfonsi,[4] L. Althueser,[5] F. D. Amaro,[6] V. C. Antochi,[2] E. Angelino,[7] F. Arneodo,[8] D. Barge,[2] L. Baudis,[9] B. Bauermeister,[2] L. Bellagamba,[3] M. L. Benabderrahmane,[8] T. Berger,[10] P. A. Breur,[11] A. Brown,[9] E. Brown,[10] S. Bruenner,[12] G. Bruno,[8] R. Budnik,[13] C. Capelli,[9] J. M. R. Cardoso,[6] D. Cichon,[12] D. Coderre,[14] A. P. Colijn,[11, *] J. Conrad,[2] J. P. Cussonneau,[15] M. P. Decowski,[11] P. de Perio,[1] A. Depoian,[16] P. Di Gangi,[3] A. Di Giovanni,[8] S. Diglio,[15] A. Elykov,[14] G. Eurin,[12] J. Fei,[17] A. D. Ferella,[2] A. Fieguth,[5] W. Fulgione,[18, 7] P. Gaemers,[11] A. Gallo Rosso,[18] M. Galloway,[9] F. Gao,[1] M. Garbini,[3] L. Grandi,[19] Z. Greene,[1] C. Hasterok,[12] C. Hils,[4] E. Hogenbirk,[11] J. Howlett,[1] M. Iacovacci,[20] R. Itay,[13] F. Joerg,[12] S. Kazama,[21, †] A. Kish,[9] M. Kobayashi,[1] G. Koltman,[13] A. Kopec,[16] H. Landsman,[13] R. F. Lang,[16] L. Levinson,[13] Q. Lin,[1, ‡] S. Lindemann,[14] M. Lindner,[12] F. Lombardi,[6, 17] J. A. M. Lopes,[6, §] E. López Fune,[22] C. Macolino,[23] J. Mahlstedt,[2] M. Manenti,[8] A. Manfredini,[9, 13] F. Marignetti,[20] T. Marrodán Undagoitia,[12] J. Masbou,[15] S. Mastroianni,[20] M. Messina,[18, 8] K. Micheneau,[15] K. Miller,[19] A. Molinario,[18] K. Morå,[2] Y. Mosbacher,[13] M. Murra,[5] J. Naganoma,[18, 24] K. Ni,[17] U. Oberlack,[4] K. Odgers,[10] J. Palacio,[15] B. Pelssers,[2] R. Peres,[9] J. Pienaar,[19] V. Pizzella,[12] G. Plante,[1] R. Podviianiuk,[18] J. Qin,[16] H. Qiu,[13] D. Ramírez García,[14] S. Reichard,[9] B. Riedel,[19] A. Rocchetti,[14] N. Rupp,[12] J. M. F. dos Santos,[6] G. Sartorelli,[3] N. Šarčević,[14] M. Scheibelhut,[4] S. Schindler,[4] J. Schreiner,[12] D. Schulte,[5] M. Schumann,[14] L. Scotto Lavina,[22] M. Selvi,[3] P. Shagin,[24] E. Shockley,[19] M. Silva,[6] H. Simgen,[12] C. Therreau,[15] D. Thers,[15] F. Toschi,[14] G. Trinchero,[7] C. Tunnell,[24] N. Upole,[19] M. Vargas,[5] G. Volta,[9] O. Wack,[12] H. Wang,[25] Y. Wei,[17] C. Weinheimer,[5] D. Wenz,[4] C. Wittweg,[5] J. Wulf,[9] J. Ye,[17] Y. Zhang,[1] T. Zhu,[1] and J. P. Zopounidis[22]

(XENON Collaboration)[¶]

[1] *Physics Department, Columbia University, New York, NY 10027, USA*
[2] *Oskar Klein Centre, Department of Physics, Stockholm University, AlbaNova, Stockholm SE-10691, Sweden*
[3] *Department of Physics and Astronomy, University of Bologna and INFN-Bologna, 40126 Bologna, Italy*
[4] *Institut für Physik & Exzellenzcluster PRISMA, Johannes Gutenberg-Universität Mainz, 55099 Mainz, Germany*
[5] *Institut für Kernphysik, Westfälische Wilhelms-Universität Münster, 48149 Münster, Germany*
[6] *LIBPhys, Department of Physics, University of Coimbra, 3004-516 Coimbra, Portugal*
[7] *INAF-Astrophysical Observatory of Torino, Department of Physics,*
University of Torino and INFN-Torino, 10125 Torino, Italy
[8] *New York University Abu Dhabi, Abu Dhabi, United Arab Emirates*
[9] *Physik-Institut, University of Zurich, 8057 Zurich, Switzerland*
[10] *Department of Physics, Applied Physics and Astronomy, Rensselaer Polytechnic Institute, Troy, NY 12180, USA*
[11] *Nikhef and the University of Amsterdam, Science Park, 1098XG Amsterdam, Netherlands*
[12] *Max-Planck-Institut für Kernphysik, 69117 Heidelberg, Germany*
[13] *Department of Particle Physics and Astrophysics, Weizmann Institute of Science, Rehovot 7610001, Israel*
[14] *Physikalisches Institut, Universität Freiburg, 79104 Freiburg, Germany*
[15] *SUBATECH, IMT Atlantique, CNRS/IN2P3, Université de Nantes, Nantes 44307, France*
[16] *Department of Physics and Astronomy, Purdue University, West Lafayette, IN 47907, USA*
[17] *Department of Physics, University of California, San Diego, CA 92093, USA*
[18] *INFN-Laboratori Nazionali del Gran Sasso and Gran Sasso Science Institute, 67100 L'Aquila, Italy*
[19] *Department of Physics & Kavli Institute for Cosmological Physics, University of Chicago, Chicago, IL 60637, USA*
[20] *Department of Physics "Ettore Pancini", University of Napoli and INFN-Napoli, 80126 Napoli, Italy*
[21] *Kobayashi-Maskawa Institute for the Origin of Particles and the Universe,*
Nagoya University, Furo-cho, Chikusa-ku, Nagoya, Aichi 464-8602, Japan
[22] *LPNHE, Université Pierre et Marie Curie, Université Paris Diderot, CNRS/IN2P3, Paris 75252, France*
[23] *LAL, Université Paris-Sud, CNRS/IN2P3, Université Paris-Saclay, F-91405 Orsay, France*
[24] *Department of Physics and Astronomy, Rice University, Houston, TX 77005, USA*
[25] *Physics & Astronomy Department, University of California, Los Angeles, CA 90095, USA*
(Dated: October 7, 2019)

Direct dark matter detection experiments based on a liquid xenon target are leading the search for dark matter particles with masses above $\sim 5\,\text{GeV/c}^2$, but have limited sensitivity to lighter masses because of the small momentum transfer in dark matter-nucleus elastic scattering. However, there is an irreducible contribution from inelastic processes accompanying the elastic scattering, which leads to the excitation and ionization of the recoiling atom (the Migdal effect) or the emission of a Bremsstrahlung photon. In this letter, we report on a probe of low-mass dark matter with masses down to about $85\,\text{MeV/c}^2$ by looking for electronic recoils induced by the Migdal effect and

Bremsstrahlung, using data from the XENON1T experiment. Besides the approach of detecting both scintillation and ionization signals, we exploit an approach that uses ionization signals only, which allows for a lower detection threshold. This analysis significantly enhances the sensitivity of XENON1T to light dark matter previously beyond its reach.

The existence of dark matter (DM) is supported by various astronomical and cosmological observations [1–3] but its nature remains unknown. The most promising DM candidate is the so-called weakly interacting massive particle (WIMP) [4], which explains the current abundance of dark matter as a thermal relic of the Big Bang [5]. In the last three decades, numerous terrestrial experiments have been built to detect the faint interactions between WIMPs and ordinary matter. Among them, experiments using dual-phase (liquid/gas) xenon time projection chambers (TPCs) [6–8] are leading the search for WIMPs with masses from a few GeV/c^2 to TeV/c^2. The mass of the WIMP is expected to be larger than about $2\,\text{GeV/c}^2$ from the Lee-Weinberg limit [5] assuming a weak scale interaction. On the other hand, DM in the sub-GeV/c^2 mass range has more recently been proposed in several models [9]. In this letter, we report on a probe of light DM-nucleon elastic interactions by looking for electronic recoils (ERs) in XENON1T, induced by secondary radiation (Bremsstrahlung [10] and the Migdal effect [11, 12]) that can accompany a nuclear recoil (NR). ER signals induced by the Migdal effect and Bremsstrahlung (BREM) can go well below 1 keV, where the detection efficiency for scintillation signal is low. Therefore, in addition to the analysis utilizing both ionization and scintillation signals, we performed analysis using the ionization signal only, which improves the detection efficiency for sub-keV ER events. We present results from a proble of light DM (LDM) with masses as low as 85 MeV/c^2.

The XENON1T direct dark matter detection experiment [13] uses a dual-phase TPC containing 2 tonnes of ultra-pure liquid xenon (LXe) as the active target material. It is located at the INFN Laboratori Nazionali del Gran Sasso (LNGS) in Italy, which has an average rock overburden of 3600 m water-equivalent. The prompt primary scintillation (S1) and secondary electroluminescence of ionized electrons (S2) signals are detected by top and bottom arrays of 248 Hamamatsu R11410-21 3″ photomultiplier tubes (PMTs) [14, 15]. They are used to reconstruct the deposited energy and the event interaction position in three dimensions, which allows for fiducialization of the active volume [16, 17]. The XENON1T experiment has published WIMP search results by looking for NRs from WIMP-nucleus elastic scattering using data from a one-tonne-year exposure, achieving the lowest ER background in a DM search experiment [8]. The excellent sensitivity of LXe experiments to heavy WIMPs comes from the heavy xenon nucleus which gives a coherent enhancement of the interaction cross-section and from the large NR energy. The sensitivity to sub-GeV/c^2 LDM, on the other hand, decreases rapidly with lowering DM mass since detectable scintillation and ionization signals produced by these NRs become too small. The energy threshold (defined here as the energy at which the efficiency is 10%) in a LXe TPC is mainly limited by the amount of detectable S1 signals. A significant fraction of deposited NR energy is transferred into heat due to the Lindhard quenching effect [18]. Thus the detection efficiency for these NRs becomes extremely low, with less than 10% for NRs below 3.5 keV in XENON1T [8]. It is challenging to detect the NR signals from LDM interactions.

Unlike NRs, ERs lose negligible energy as heat because recoil electrons have small masses compared with xenon nuclei. This leads to a lower energy threshold for ER signals. Probing the ER signals induced by the Migdal effect and BREM enables a significant boost of XENON1T's sensitivity to LDMs, thanks to the lowered threshold.

When a particle elastically scatters off a xenon nucleus, the nucleus undergoes a sudden momentum change with respect to the orbital atomic electrons, resulting in the polarization of the recoiling atom and a kinematic boost of the electrons. The de-polarization process can lead to BREM emission [10], and the kinematic boost of atomic electrons can result in ionization and/or excitation of the atom, which eventually causes secondary radiation, known as the Migdal effect (MIGD) [11, 12].

The differential rate of BREM emission with photon energy E_{ER} is given by

$$\frac{d^2R}{dE_{\text{ER}}dv} \propto \frac{|f(E_{\text{ER}})|^2}{E_{\text{ER}}}\sqrt{1 - \frac{2E_{\text{ER}}}{\mu_N v^2}}\left(1 - \frac{E_{\text{ER}}}{\mu_N v^2}\right), \quad (1)$$

where v, μ_N, and $f(E_{\text{ER}})$ are the velocity of DM, the reduced mass of the xenon nucleus and DM, and the atomic scattering factor, respectively [10].

The differential rate of MIGD process giving an NR of energy E_{NR} accompanied by an ER of energy E_{ER} is given by

$$\begin{aligned}\frac{dR}{dE_{\text{ER}}} &\simeq \int dE_{\text{NR}}dv\frac{d^2R}{dE_{\text{NR}}dv}\\&\times \frac{1}{2\pi}\sum_{n,l}\frac{d}{dE_{\text{ER}}}p_{q_e}^c(n, l \to E_{\text{ER}} - E_{n,l}),\end{aligned} \quad (2)$$

where $p_{q_e}^c$ is the probability for an atomic electron, with quantum numbers (n, l) and binding energy $E_{n,l}$, to be ionized and receive a kinetic energy $E_{ER} - E_{n,l}$ [12]. $p_{q_e}^c$ is related to q_e which is the momentum of each electron in the rest frame of the nucleus after the scattering. The shell vacancy is immediately refilled, and an X-ray or an Auger electron with energy $E_{n,l}$ is emitted. $E_{n,l}$ is measured simultaneously with the energy deposited by the ionized electron, since the typical timescale of the de-excitation process is $\mathcal{O}(10)$ fs. Atomic electrons can also undergo excitation instead of ionization, in which case an X-ray is emitted during de-excitation [12]. Excitation, however, is sub-dominant compared to the ionization process, and thus is not considered in this analysis. Only the contributions from the ionization of M-shell ($n=3$) and N-shell ($n=4$) electrons are considered in this work, as inner electrons ($n \leq 2$) are too strongly bound to the nucleus to contribute significantly. The contribution from the ionization of valence electrons ($n=5$) is neglected because it is subdominant in region of interest compared to the ones from M- and N-shell electrons, and the calculation of it has large uncertainty since the assumption of isolated atom is used for LXe [12]. An illustration of MIGD and BREM is given in Fig. 1. The radiation from MIGD is typically 3-4 orders of magnitude more likely to occur than BREM. Although only a very small fraction (about 3×10^{-8} and 8×10^{-6} for DM masses of 0.1 and 1.0 GeV/c^2, respectively) of NRs accompanies MIGD radiations, the larger energy and ER nature make them easier to be detected than the pure NRs.
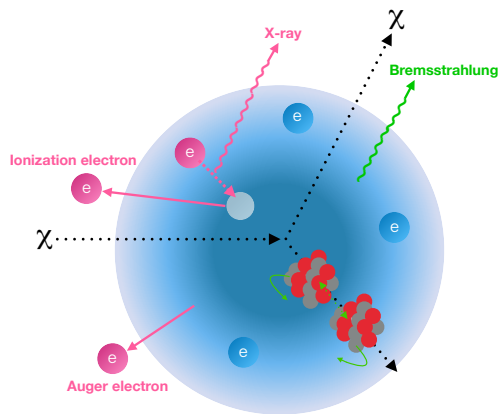

FIG. 1. Illustration of the ER signal production from BREM (green) and MIGD processes (pink) after elastic scattering between DM (χ) and a xenon nucleus. The electrons illustrated in pink represent those involved in ionization, de-excitation, and Auger electron emission during a MIGD process.

The data used in previous analyses [8] consists of two science runs with a livetime of 32.1 days (SR0) and 246.7 days (SR1), respectively. The two runs were taken under slightly different detector conditions. To maximize the amount of data acquired under stable detector conditions

we decided to use SR1 only. The same event selection, fiducial mass, correction, and background models as described in [8] are used for the SR1 data, which we refer to as the S1-S2 data in later text. The exposure of the S1-S2 data is about 320 tonne-days. The interpretation of such S1-S2 analysis is based on the corrected S1 (cS1) signal and the corrected S2 signal from the PMTs at the bottom of the TPC (cS2$_b$).
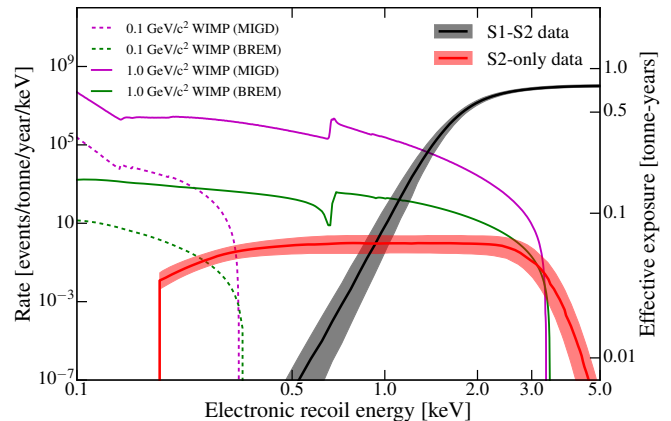

FIG. 2. Median effective exposures of ER signals after event selections as a function of recoil energy for the S1-S2 data (black line) and S2-only data (red line). The 68% credible regions of the effective exposures are also shown as the shaded regions. The expected event rate of DM-nucleus scattering from MIGD/BREM for DM masses of 0.1 and 1.0 GeV/c^2 are overlaid as well, in magenta/green dashed and solid lines, respectively, assuming a spin-independent DM-nucleon interaction cross section of 10^{-35} cm^2.

The region of interest in the S1-S2 data is from 3 to 70 photoelectrons (PEs) in cS1, which corresponds to median ER energies from 1.4 to 10.6 keV in the 1.3-tonne fiducial volume (FV) of XENON1T. The lower value is dictated by the requirement of the 3-fold PMT coincidence for defining a valid S1 signal [16]. A detailed signal response model [17] is used to derive the influence of various detector features, including the requirement of the 3-fold PMT coincidence, on the reconstructed signals. The effective exposure, which is defined as exposure times detection efficiency, and its uncertainty as a function of deposited ER energy for the S1-S2 data are shown in Fig. 2, with the signal spectra from MIGD and BREM induced by 0.1 GeV/c^2 and 1 GeV/c^2 DM masses overlaid. The (cS2$_b$, cS1) distribution of S1-S2 data are shown in Fig. 3. The rise of the event rate at around 0.85 keV for DM mass of 1.0 GeV/c^2 is contributed by the ionization of M-shell electrons [10, 12]. In our signal models, deposited energy below 1 keV, at which the median detection efficiency in 1.3-tonne FV is 10%, from MIGD and BREM is neglected for the S1-S2 data in the following analysis. There are only two sub-keV measurement of ionization yield for ER in LXe [19, 20].
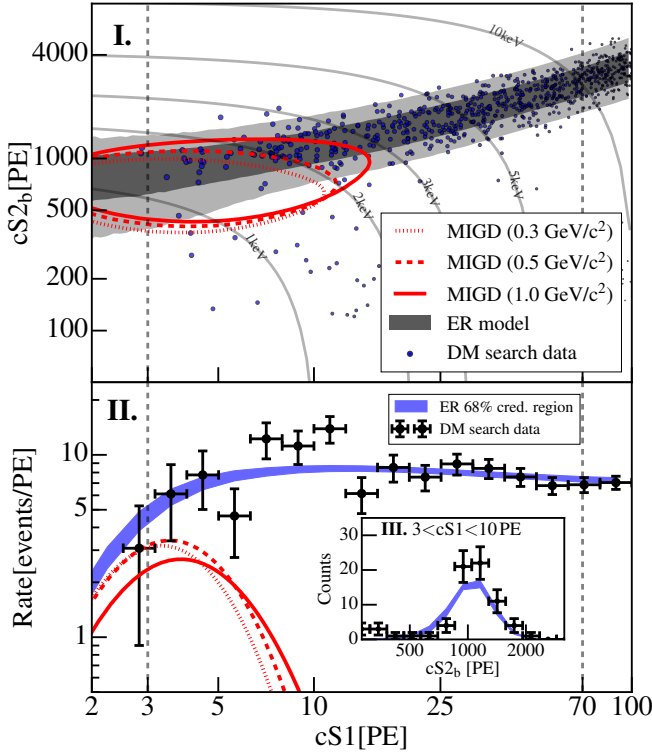
The S1-S2 data selections [16] provide excellent rejec-

FIG. 3. Comparison of cS1 and $cS2_b$ spectra between the S1-S2 data and the signal response model [17]. In the upper panel (I), the distribution of the S1-S2 data in $(cS2_b, cS1)$ space is shown as light blue dots, along with the best-fit ER background model (black shaded region). The contours containing 90% of the expected signals from MIGD for 0.3, 0.5, and $1\,\mathrm{GeV/c^2}$ DM are shown in red dotted, dashed, and solid lines, respectively. Gray lines show isoenergy contours in ER energy. The events having lower $cS2_b$ than what we expect for ER are mostly surface backgrounds [8], which have minimal impact to the results of this study. The lower panel (II) shows the projected cS1 distribution of the S1-S2 data, where $cS2_b$ is within the 2σ contour of ER model shown in panel (I). For comparision, the 68% credible region of cS1 distribution from ER background model (blue shadow) is shown, which is mainly attributed to the systematic uncertainties of the model. The cS1 distributions of the expected signals from MIGD for 0.3, 0.5, and $1\,\mathrm{GeV/c^2}$ DM with assumed spin-independent DM-nucleon cross sections of 2×10^{-28}, 10^{-36}, and 10^{-38} cm^2, respectively, are shown as well. The vertical dashed lines indicate the region of interest (3-70 PE). The inset, panel (III) shows the $cS2_b$ distribution, with cS1 in (3, 10) PE, compared with the 68% credible region of the $cS2_b$ spectra from the ER background model (blue shadow).
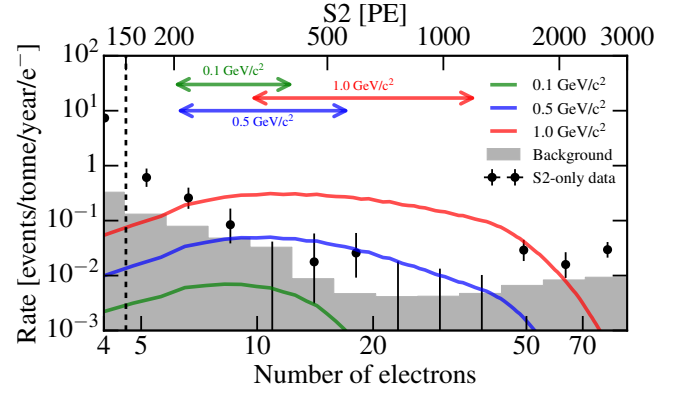

FIG. 4. Observed S2 spectra for the S2-only data after the optimized selection described in [21]. The expected spectra of ER signals induced by MIGD for DM with mass of 0.1, 0.5, and $1.0\,\mathrm{GeV/c^2}$ are shown in green, blue, and red solid lines, respectively, assuming the spin-independent DM-nucleon interaction cross section of $10^{-33}\,\mathrm{cm^2}$ for $0.1\,\mathrm{GeV/c^2}$ DM and of $10^{-35}\,\mathrm{cm^2}$ for 0.5 and $1.0\,\mathrm{GeV/c^2}$ DM. The gray shaded region shows the conservative background model used in analysis of S2-only data. The arrows indicate the S2 ROIs that are later used in inference for the three DM signals above-mentioned. The S2 threshold used for the S2-only data is denoted in the dashed black line.

tion of noise and backgrounds, and are characterized as well by the well-established background models [17] and a fully blind analysis [8]. However they also limit the detection efficiency of $\mathcal{O}(1)$ keV energy depositions. We therefore consider also the events with no specific requirement on S1 (S2-only data) in this work. Although the reduction of available information in the S2-only data implies less background discrimination, the increased detec-

tion efficiency in the $< 1\,\mathrm{keV}$ ER energy region, shown in Fig. 2, enables a more sensitive search for LDM-nucleus interactions through MIGD and BREM. The interpretation of such S2-only data is based on the uncorrected S2 signal, combining both signals from top and bottom PMT arrays.

We analyze the S2-only data as in [21], using the LDM signal models appropriate for MIGD and BREM. As detailed in [21], 30% of the data was used for choosing regions of interest (ROIs) in S2 and event selections. A different S2 ROI is chosen for each dark matter model and mass to maximize the signal-to-noise ratio, based on the training data. The event selections used for this work are the same as in [21], and mainly based on the width of each S2 waveform, reconstructed radius, and PMT hit-pattern of the S2. Fig. 4 shows the observed S2 spectra for the S2-only data, along with the expected DM signal distributions by MIGD with masses of 0.1, 0.5, and $1.0\,\mathrm{GeV/c^2}$, respectively. The S2 ROIs for these three DM models shown in Fig. 4 are indicated by the colored arrows. Conservative estimates of the background from ^{214}Pb-induced β decays, solar-neutrino induced NRs, and surface backgrounds from the cathode electrode are used in the inference [21]. The background model is shown in Fig. 4 as shaded gray region.

The detector response to ERs from MIGD and BREM in $(cS2_b, cS1)$ space (for the S1-S2 data) and in reconstructed number of electrons (for the S2-only data) is derived using the signal response model described in [17]. Note that the ionization yield used for the S2-only data

is more conservative than the Noble Element Simulation Technique (NEST) v2 model [22]. Fig. 3 shows the comparison between the expectation from our signal response model and the S1-S2 data, as well as the ($cS2_b$, cS1) distribution of ERs from MIGD. Signal contours for different DM masses are similar since the energy spectra from MIGD and BREM are not sensitive to incident dark matter velocity as long as it is kinematically allowed. We have ignored the contribution of NRs in the signal model of MIGD and BREM, since it is small compared with ERs from MIGD and BREM in this analysis and there is no measurement of scintillation and ionization yields in LXe for simultaneous ER and NR energy depositions. We use the inference only for DM mass below $2\,\mathrm{GeV}/c^2$, above which the contribution of an NR in the signal rate becomes comparable with or exceeds the signal model uncertainty.

The S1-S2 data are interpreted using an unbinned profile likelihood ratio as the test statistic, as detailed in [17]. The unbinned profile likelihood is calculated using background models defined in $cS2_b$, cS1, and spatial coordinates. The uncertainties from the scintillation and ionization yields of ER backgrounds, along with the uncertainties in the estimated rates of each background component, are taken into account in the inference [17]. The inference procedure for the S2-only data is detailed in [21], which is based on simple Poisson statistics using the number of events in the S2 ROI. The event rates of spin-independent (SI) and -dependent (SD) DM-nucleon elastic scattering are calculated following the approaches described in [8, 32] and [33], respectively.

The results are also interpreted in a scenario where LDM interacts with the nucleon through a scalar force mediator ϕ with equal effective couplings to the proton and neutron as in the SI DM-nucleon elastic scattering. In this scenario, the differential event rates are corrected by $m_\phi^4/(m_\phi^2 + q^2/c^2)^2$ [34, 35], where $q = \sqrt{2m_N E_R}$ and m_N are the momentum transfer and the nuclear mass, respectively. We take the light mediator (LM) regime where the momentum transfer is much larger than m_ϕ and thus the interaction cross section scales with m_ϕ^4. In this regime, the contribution of NRs is largely suppressed compared with SI DM-nucleon elastic scattering due to the long-range nature of the interaction. Therefore, the results are interpreted for DM mass up to 5 GeV/c^2 for SI-LM DM-nucleon elastic scattering.

In addition, we also take into account the fact that DM particle may be stopped or scatter multiple times when passing through Earth's atmosphere, mantle, and core before reaching the detector (Earth-shielding effect) [36–38]. If the DM-matter interaction is sufficiently strong, the sensitivity for detecting such DM particles in terrestrial detectors, especially in underground laboratory, can be reduced or even lost totally. Following [24], *verne* code [39] is used to calculate the Earth-shielding effect for SI DM-nucleon interaction. A modification of the
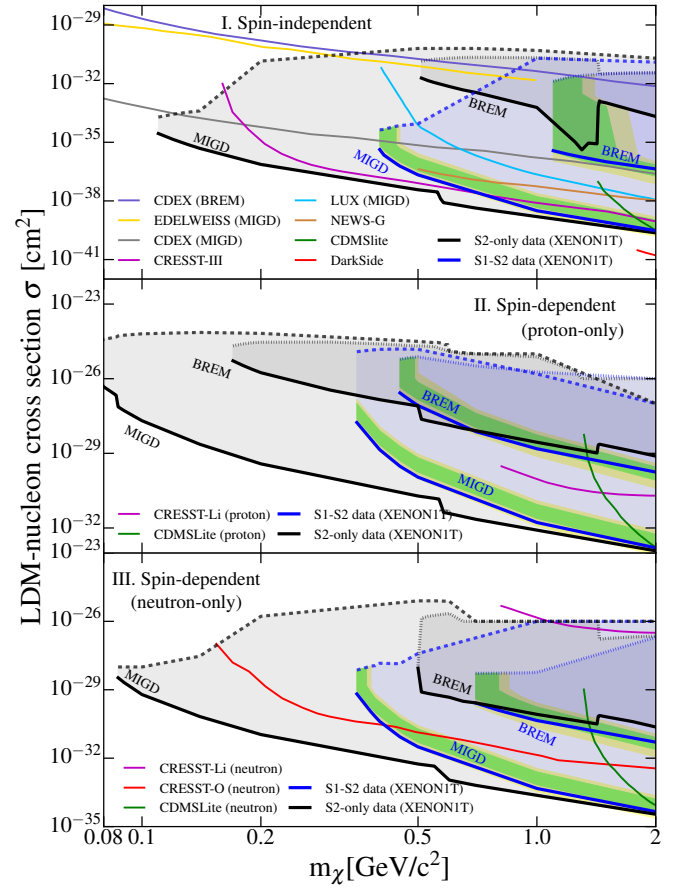

FIG. 5. Limits on the SI (upper panel), SD proton-only (middle panel), and SD neutron-only (lower panel) DM-nucleon interaction cross-sections at 90% C.L. using signal models from MIGD and BREM in the XENON1T experiment with the S1-S2 data (blue contours and lines) and S2-only data (black contours and lines). The solid and dashed (dotted) lines represent the lower boundaries (also referred to as upper limits) and MIGD (BREM) upper boundaries of the excluded parameter regions. Green and yellow shaded regions give the 1 and $2\,\sigma$ sensitivity contours for upper limits derived using the S1-S2 data, respectively. The upper limits on the SI DM-nucleon interaction cross sections from LUX [23], EDELWEISS [24], CDEX [25], CRESST-III [26], NEWS-G [27], CDMSLite-II [28], and DarkSide-50 [29], and upper limits on the SD DM-nucleon interaction cross sections from CRESST [26, 30] and CDMSLite [31] are also shown. Note that the limits derived using the S1-S2 and S2-only data are inferred using unbinned profile likelihood method [16] and simple Poisson statistics with the optimized event selection [21], respectively. The sensitivity contours for the S2-only data is not given since the background models used in the S2-only data are conservative [21].

verne code based on the methodology in [40] is applied for the calculations of SD and SD-LM DM-nucleon interactions. To account for the Earth-shielding effect for SD DM-nucleon interaction, ^{14}N in the atmosphere and ^{29}Si in Earth's mantle and core are considered, and their spin expectation values, $\langle S_n \rangle$ and $\langle S_p \rangle$, are taken from [41].

Both the lower and upper boundaries of excluded parameter space are reported in this work. The lower boundaries are conventionally referred to as upper limits in later context, and are the primary interest of this work. The upper boundaries are dominated by the overburden configuration of the Gran Sasso laboratory which hosts the detector.
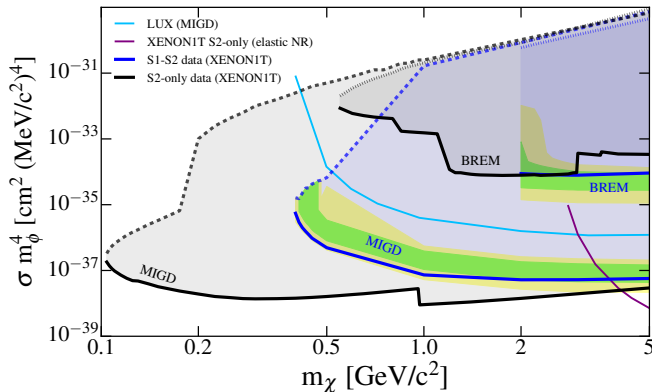

FIG. 6. Limits on the SI-LM DM-nucleon interaction cross-sections at 90% C.L. using signal models from MIGD and BREM in the XENON1T experiment with the S1-S2 data (blue contours and lines) and S2-only data (black contours and lines). The figure description is the same as in Fig. 5. The upper limits on the SI DM-nucleon interaction cross sections from LUX [23] and XENON1T S2-only (elastic NR results) [21] are also shown.

No significant excess is observed above the background expectation in the search using the S1-S2 data. Fig. 5 shows the 90% confidence-level (C.L.) limits on the SI and SD (proton-only and neutron-only cases) DM-nucleon interaction cross-section using signal models from MIGD and BREM with masses from about $85\,\mathrm{MeV/c^2}$ to $2\,\mathrm{GeV/c^2}$, and Fig. 6 shows the 90% C.L. limits on the SI-LM DM-nucleon interaction cross-section with masses from about $100\,\mathrm{MeV/c^2}$ to $5\,\mathrm{GeV/c^2}$. The sensitivity contours for the results derived using S2-only data are not shown because of the conservativeness of the background model. The upper limits derived using the S1-S2 data deviate from the median sensitivity by about 1-2 σ due to the under-fluctuation of the ER background in the low energy region. As described in [21], the jumps in the S2-only limits are originating from changes in the observed number of events due to the mass-dependent S2 ROIs. The results, by searching for ER signals induced by MIGD, give the best lower exclusion boundaries on SI, SD proton-only, SD neutron-only, and SI-LM DM-nucleon interaction cross-section for mass below about 1.8, 2.0, 2.0, and $4.0\,\mathrm{GeV/c^2}$, respectively as compared to previous experiments [23–31]. The upper limits derived from the S1-S2 data become comparable with those from the S2-only data at $\sim\mathrm{GeV/c^2}$ since the efficiency of the S1-S2 data to DM signals with mass of

$\sim\mathrm{GeV/c^2}$ becomes sufficiently high. However, the upper limits derived from the S1-S2 data do not provide significantly better constraints than those from the S2-only data for DM masses larger than $1\,\mathrm{GeV/c^2}$, because both data are dominated by the ER background, which is very similar to the expected DM signal.

In summary, we performed a search for LDM by probing ER signals induced by MIGD and BREM, using data from the XENON1T experiment. These new detection channels significantly enhance the sensitivity of LXe experiments to masses unreachable in the standard NR searches. We set the most stringent upper limits on the SI and SD DM-nucleon interaction cross-sections for masses below $1.8\,\mathrm{GeV/c^2}$ and $2\,\mathrm{GeV/c^2}$, respectively. Together with the standard NR search [8], XENON1T results have reached unprecedented sensitivities to both low-mass (sub-$\mathrm{GeV/c^2}$) and high-mass ($\mathrm{GeV/c^2}$ - $\mathrm{TeV/c^2}$) DM. With the upgrade to XENONnT, we expect to further improve the sensitivity to DM with masses ranging from about $85\,\mathrm{MeV/c^2}$ to beyond a $\mathrm{TeV/c^2}$.

* Also at Institute for Subatomic Physics, Utrecht University, Utrecht, Netherlands

† kazama@isee.nagoya-u.ac.jp

‡ ql2265@vip.163.com

§ Also at Coimbra Polytechnic - ISEC, Coimbra, Portugal

¶ xenon@lngs.infn.it

[1] D. Clowe, A. Gonzalez, and M. Markevitch, ApJ **604**, 596 (2004).

[2] V. C. Rubin, W. K. Ford Jr, and N. Thonnard, ApJ **238**, 471 (1980).

[3] N. Aghanim *et al.* (Planck), arXiv:1807.06209 (2018).

[4] G. Jungman, M. Kamionkowski, and K. Griest, Phys. Rept. **267**, 195 (1996).

[5] B. W. Lee and S. Weinberg, Phys. Rev. Lett. **39**, 165 (1977).

[6] D. S. Akerib *et al.* (LUX), Phys. Rev. Lett. **116**, 161302 (2016).

[7] X. Cui *et al.* (PandaX-II), Phys. Rev. Lett. **119**, 181302 (2017).

[8] E. Aprile *et al.* (XENON), Phys. Rev. Lett. **121**, 111302 (2018).

[9] M. Battaglieri *et al.*, arXiv:1707.04591 (2017).

[10] C. Kouvaris and J. Pradler, Phys. Rev. Lett. **118**, 031803 (2017).

[11] A. B. Migdal, J. Phys.(USSR) **4**, 449 (1941).

[12] M. Ibe, W. Nakano, Y. Shoji, and K. Suzuki, JHEP **03**, 194 (2018).

[13] E. Aprile *et al.* (XENON), Eur. Phys. J. C **77**, 881 (2017).

[14] E. Aprile *et al.* (XENON), Eur. Phys. J. C **75**, 546 (2015).

[15] E. Aprile *et al.* (XENON), JINST **12**, no. 01, P01024 (2017).

[16] E. Aprile *et al.* (XENON), arXiv: 1906.04717 (2019).

[17] E. Aprile *et al.* (XENON), Phys. Rev. D **99**, 112009 (2019).

[18] J. Lindhard, V. Nielsen, M. Scharff, and P. Thomsen, Mat. Fys. Medd. Dan. Vid. Selsk **33**, 1 (1963).

[19] D. S. Akerib *et al.* (LUX), Phys. Rev. D **96**, 112011 (2017).

[20] E. Boulton, E. Bernard, N. Destefano, B. Edwards, M. Gai, S. Hertel, M. Horn, N. Larsen, B. Tennyson, C. Wahl, *et al.*, Journal of Instrumentation **12**, P08004 (2017).

[21] E. Aprile *et al.* (XENON), arXiv: 1907.11485 (2019).

[22] M. Szydagis *et al.*, "Noble element simulation technique v2.0," (2018).

[23] D. S. Akerib *et al.* (LUX), Phys. Rev. Lett. **122**, 131301 (2019).

[24] E. Armengaud *et al.* (EDELWEISS), Phys. Rev. D **99**, 082003 (2019).

[25] Z. Z. Liu *et al.* (CDEX), arXiv:1905.00354 (2019).

[26] A. Abdelhameed *et al.* (CRESST), arXiv:1904.00498 (2017).

[27] Q. Arnaud *et al.* (NEWS-G), Astropart. Phys. **97**, 54 (2018).

[28] R. Agnese *et al.* (SuperCDMS), Phys. Rev. Lett. **116**, 071301 (2016).

[29] P. Agnes *et al.* (DarkSide), Phys. Rev. Lett. **121**, 081307 (2018).

[30] A. Abdelhameed *et al.* (CRESST), arXiv:1902.07587 (2019).

[31] R. Agnese *et al.* (CDMS), Phys. Rev. D **97**, 022002 (2018).

[32] J. Lewin and P. Smith, Astropart. Phys. **6**, 87 (1996).

[33] E. Aprile *et al.* (XENON), Phys. Rev. Lett. **122**, 141301 (2019).

[34] E. Del Nobile, M. Kaplinghat, and H. B. Yu, JCAP **1510**, 055 (2015).

[35] X. Ren *et al.* (PandaX-II), Phys. Rev. Lett. **121**, 021304 (2018).

[36] T. Emken and C. Kouvaris, Phys. Rev. D **97**, 115047 (2018).

[37] M. S. Mahdawi and G. R. Farrar, arXiv:1712.01170 (2017).

[38] T. Emken and C. Kouvaris, JCAP **2017**, 031 (2017).

[39] B. J. Kavanagh, "bradkav/verne: Release," (2017).

[40] B. J. Kavanagh, Phys. Rev. D **97**, 123013 (2018).

[41] D. Hooper and S. D. McDermott, Phy. Rev. D **97**, 115006 (2018).